Full length article

Monitoring matrix remodeling in the cellular microenvironment using microrheology for complex cellular systems

Johanna Hafner[a,*], David Grijalva[a], Anita Ludwig-Husemann[b,c], Sarah Bertels[d], Lea Bensinger[a], Annamarija Raic[b,c], Julian Gebauer[e], Claude Oelschlaeger[a], Martin Bastmeyer[b,d], Karen Bieback[e], Cornelia Lee-Thedieck[b,c], Norbert Willenbacher[a]

[a] *Institute of Mechanical Process Engineering and Mechanics, Applied Mechanics Group, Karlsruhe Institute of Technology, 76137 Karlsruhe, Germany*
[b] *Institute of Functional Interfaces, Karlsruhe Institute of Technology, 76344 Eggenstein-Leopoldshafen, Germany*
[c] *Institute of Cell Biology and Biophysics, Department of Cell Biology, Leibniz University Hannover, 30419 Hannover, Germany*
[d] *Department of Cell- and Neurobiology, Zoological Institute, Karlsruhe Institute of Technology, 76137 Karlsruhe, Germany*
[e] *Institute of Transfusion Medicine and Immunology, Medical Faculty Mannheim, Heidelberg University, German Red Cross Blood Service Baden-Württemberg - Hessen, 68167 Mannheim, Germany*

ARTICLE INFO

Keywords:
Multiple particle tracking
ECM elasticity
Mesenchymal stem cell differentiation
HUVECs
Micromechanics
MMP inhibitor

ABSTRACT

Multiple particle tracking (MPT) microrheology was employed for monitoring the development of extracellular matrix (ECM) mechanical properties in the direct microenvironment of living cells. A customized setup enabled us to overcome current limitations: (i) Continuous measurements were enabled using a cell culture chamber, with this, matrix remodeling by fibroblasts in the heterogeneous environment of macroporous scaffolds was monitored continuously. (ii) Employing tracer laden porous scaffolds for seeding human mesenchymal stem cells (hMSCs), we followed conventional differentiation protocols. Thus, we were, for the first time able to study the massive alterations in ECM elasticity during hMSC differentiation. (iii) MPT measurements in 2D cell cultures were enabled using a long distance objective. Exemplarily, local mechanical properties of the ECM in human umbilical vein endothelial cell (HUVEC) cultures, that naturally form 2D layers, were investigated scaffold-free.

Using our advanced setup, we measured local, apparent elastic moduli $G_{0,app}$ in a range between 0.08 and 60 Pa. For fibroblasts grown in collagen-based scaffolds, a continuous decrease of local matrix elasticity resulted during the first 10 hours after seeding. The osteogenic differentiation of hMSC cells cultivated in similar scaffolds, led to an increase of $G_{0,app}$ by 100 %, whereas after adipogenic differentiation it was reduced by 80 %. The local elasticity of ECM that was newly secreted by HUVECs increased significantly upon addition of protease inhibitor and in high glucose conditions even a twofold increase in $G_{0,app}$ was observed.

The combination of these advanced methods opens up new avenues for a broad range of investigations regarding cell-matrix interactions and the propagation of ECM mechanical properties in complex biological systems.

Statement of Significance

Cells sense the elasticity of their environment on a micrometer length scale. For studying the local elasticity of extracellular matrix (ECM) in the direct environment of living cells, we employed an advanced multiple particle tracking microrheology setup. MPT is based on monitoring the Brownian motion of tracer particles, which is restricted by the surrounding network. Network elasticity can thus be quantified.

Overcoming current limitations, we realized continuous investigations of ECM elasticity during fibroblast growth. Furthermore, MPT measurements of stem cell ECM showed ECM stiffening during osteogenic differentiation and softening during adipogenic differentiation. Finally, we characterized small amounts of delicate ECM newly secreted in scaffold-free cultures of endothelial cells, that naturally form 2D layers.

* Corresponding author.
E-mail address: johanna.roether@kit.edu (J. Hafner).

1. Introduction

Many cellular processes, such as motility, differentiation, adhesion, proliferation and metabolism of cells depend on the mechanical properties of the extracellular matrix (ECM) [1–10], making a sound mechanical characterization of the cellular surrounding indispensable to ultimately understand and control these cellular processes. However, mechanical properties of artificial ECM substitutes and cell-secreted ECM, such as stiffness and elasticity, may alter continuously due to the impact of the cells, that live within the ECM and constantly control their environment by secreting, organizing, and remodeling matrix molecules. Thus, mechanical properties of the ECM cannot be characterized by one single value.

However, knowing the complex alteration of ECM mechanics is crucial for development of artificial ECM substitutes. Furthermore, a better understanding of cell-matrix interactions in artificial and cell-secreted ECM helps us to describe biological processes, such as wound healing, angiogenesis and cancer metastasis. E.g. tumors were shown to be highly sensitive towards mechanical stimuli from their environment and additionally cause rigorous changes in the ECM elasticity [11]. This better understanding can be achieved by monitoring the development of local mechanical properties while cells remodel their surrounding.

Traditionally, the elasticity of ECM substitutes including all types of biobased gels, was characterized in bulk experiments, such as compression and tension tests [12–16] and oscillatory shear rheometry [3,4,17–21], performed on centimeter sized specimen. These methods characterize cell-laden, potentially porous scaffolds, in some cases even flooded with liquid media with their given heterogeneity as a homogeneous material on a continuum mechanical level. This limits the explanatory power of such methods and neglects cells' sensitivity to the mechanical properties in their direct proximity that raises the need for mechanical characterization on a much shorter length-scale, i.e. less than 200 µm [22,23].

One potential approach to realize local characterization of mechanical properties is using quartz crystal microbalances, which characterize the elasticity of a nanometer thick surface layer on oscillating gold surfaces by measuring the energy dissipation [24]. Despite the high spatial resolution in vertical direction, horizontally, still the whole sensor surface, including adhering cells, ECM, and surface modifications, is considered or cells need to be removed. The latter can result in altered ECM properties. More precise localization can be achieved by using atomic force microscopy (AFM) and other indentation experiments for the characterization of the local mechanical and structural properties of biomaterials [22,25–30] and delicate natural ECM [31–33]. However, due to the indentation of a small probe, this technique is limited to probing exclusively the surface of a sample.

To circumvent these limitations, microrheology methods, in particular active microrheology methods, were employed for studying ECM substitutes. In such experiments, micrometer-sized single tracer particles or particle ensembles were placed in the cellular surrounding and their motion was actively triggered by external forces. The resulting displacement was measured, allowing for the characterization of local elasticity. For example optical tweezers were employed for studying the elasticity of ECM substitutes laden with breast cancer cells [11,34] and for the characterization of ECM elasticity in sprouting angiogenesis [35]. This latter technique has also been used to characterize changes in elastic properties of natural collagen ECM due to cellular contractility [36] and of actin filament networks due to the presence of active motors in the system [37]. It also allowed for the characterization of the heterogeneous microstructure of fibrin-based ECM [38]. Li et al. [39] used magnetic twisting beads that were conjugated to the collagen fibers of the adventitial layer of porcine aortas for studying ECM local elasticity.

Another promising optical tweezers based method is nonlinear stress inference microscopy. Using ~5 µm particles, this technique was successfully implemented for studying cell-generated stresses capable of buckling filaments in a 3D polymer matrix [40].

A gentler method to study local mechanical properties of delicate biomaterials with respect to heterogeneities on shorter length scales is passive microrheology. In contrast to active microrheology, the driving force is the Brownian motion of the tracer particles themselves and smaller tracer particles can be used.

Gambini et al. [41] used such a passive single particle tracking method for studying mechanical properties of jellyfish ECM by microscopying the jellyfish as a whole and Nijenhuis et al. [42] examined the elasticity of the pericellular matrix of chondrocytes by a combined approach of positioning the tracer particle with an optical trap and studying Brownian motion for rheological measurements.

MPT is an advanced passive microrheology technique, which allows for the characterization of the viscoelastic properties sensed by an entire particle collective ($n > 100$). Based on this, local distributions in viscoelasticity and local heterogeneity can be characterized.

MPT was initially used for characterization of intracellular elasticity [43,44] and pericellular matrix layers [45]. To our knowledge, MPT was never used for studying natural, macroporous ECM, but in several studies, ECM substitutes were characterized, including the local elasticity of artificial ECM in tumors [46] or in another approach tumor cells were encapsulated in collagen I gels, doped with particles for MPT measurements [47].

A series of MPT measurements at different time-points was used for monitoring the elasticity of special proteinase-cleavable, PEG-based ECM substitutes during several days of cell culture and revealed a decreasing matrix elasticity in the direct surrounding of encapsulated MSCs [48,49]. The decreasing matrix elasticity was explained with matrix degradation caused mainly by matrix metalloproteinases (MMPs) that were secreted by the cells. Although these approaches delivered a spatially resolved elasticity profile for defined, homogeneous materials, they possess limitations in terms of cell surroundings that can be examined: Cells need to be encapsulated in highly homogeneous PEG-based gels and the number of analyzed particles is still limited.

To overcome these restrictions, we developed a MPT protocol using macroporous collagen scaffolds of pore size ~ 50 µm and pore wall thickness ~ 5-10 µm [50] on which cells can be seeded conventionally. Cells migrate into the pores until they adhere to a pore wall and settle there. MPT measurements are thus performed in the narrow pore wall, directly in the surrounding of cells' anchoring sites. Tracer particles of very small diameter, ~ 0.2 µm, are used in order to avoid wall effects and not to disturb the gel formation. Furthermore, due to the 3D porous architecture and narrow pore wall thickness, we expect no variation of ECM mechanical properties with distance from the cell surface as well as no disturbing effect of cells contractility. For the gels investigated here, however, MPT does not yield the true bulk modulus of the gel but an apparent modulus. Values calculated from the mean square displacement of tracer particles on the basis of the generalized Stokes-Einstein (GSE) equation are much lower than bulk values (bulk results not shown here, compare [50]. This discrepancy may be due to densely crosslinked areas inaccessible for the tracer particles and thus not contributing to the MPT elasticity, or due to a pronounced contribution of stretched out of equilibrium chain segments between network junctions as observed earlier for keratin networks [51]. However, changes during cell cultivation in the apparent moduli obtained from MPT reflect changes in the mechanical properties of the ECM.

Furthermore, we combined the MPT setup with a cell culture chamber, so that continuous measurements could be performed to study the change of ECM elasticity in direct cell surrounding over time.

To validate this setup, 3T3 fibroblasts served as well characterized model system. They appear especially interesting, because maintenance of ECM properties is one key function of fibroblast cells. They are responsible for the production of ECM and its integrity, i.e. they synthesize and secrete ECM components, grouped into (i) proteoglycans and glycosaminoglycans and (ii) structural proteins, e.g. collagens and fibronectin [52]. Additionally, fibroblasts produce several classes of proteases, for example MMPs, which cleave peptide bonds in the ECM [53], as well as the corresponding inhibitors, called tissue inhibitors of metalloproteinase (TIMP) [54]. The balance of both, together with the matrix secretion, regulates ECM composition and its mechanical properties. The underlying metabolism is further regulated by the complex interplay of cell-cell and cell-matrix interactions [55].

While undifferentiated MSCs are expected to maintain and remodel the ECM properties similar to fibroblasts, differentiated MSCs change ECM mechanical properties dramatically.

During osteogenic differentiation, the expression level of collagen I and osteocalcin is increased [56]. With progressive differentiation, the formation of hydroxyapatite and mineralization of the ECM takes place [57,58].

In contrast, adipogenic differentiation is characterized by an extensive remodeling of the ECM by proteases [59,60] and is accompanied by losing cell-matrix adhesion [61]. Enzymatic degradability of the MSC's microenvironment constitutes a prerequisite for adipogenesis as well as osteogenesis [62]. Therefore, cell-matrix engineering demands a thorough understanding of cell-matrix interactions and corresponding cellular traction force change over time.

Surprisingly, the effect of cell differentiation on local matrix elasticity was never studied before, although studying the local mechanical properties of ECM substitutes and of the ECM itself appears as a very urgent question, not only in biomaterials design and cell biology, but also to uncover new therapeutic strategies. Thus, we employed MPT to study the effect of chemically induced MSC differentiation on ECM mechanical properties in 3D scaffolds.

In contrast to stromal cells forming 3D tissues, endothelial cells (ECs) are known to naturally form continuous monolayers lining the interior surface of blood vessels. For understanding their matrix elasticity, 2D models appear much more relevant than 3D studies. Consequently, we used HUVEC cells as an easily accessible model for ECs to show that MPT is even suitable to study the local elasticity of newly secreted ECM in scaffold-free 2D cell cultures.

ECs maintain a non-thrombogenic surface to facilitate blood flow and besides, they regulate the exchange of gases, nutrients, and metabolic waste between the plasma, and the interstitial spaces. In microvessels, endothelial cells can be mobilized to proliferate and migrate in response to angiogenic signals, including mechanical cues generated by the sub-endothelial ECM [63–66]. The remodeling of endothelial ECM is regulated by MMP activity. Hence, we verified this novel 2D approach by investigating the local elasticity of ECM, newly secreted by HUVECs with and without additional protease inhibitor.

In this study, we present a proof of principle for applying MPT to study local ECM elasticity. We were able to determine local shear moduli in the direct proximity of living cells and on a length scale that is relevant for cells mechanosensing. We showed the suitability and biocompatibilty of the method for three different applications, namely continuous remodeling of ECM in 3D by fibroblasts, change of ECM elasticity during differentiation of hMSCs in 3D and elasticity of newly secreted HUVEC ECM in 2D.

2. Materials and methods

2.1. 2D and 3D cell culture and differentiation

2.1.1. Scaffold preparation for 3D cell cultures

3D scaffolds were prepared as described previously [50]. In brief, 2 wt% HA (Hyaluronic acid; Contipro, Czech Republic) were dissolved in 1 % NaOH and stored for 16 h at 4°C; 4 wt% Coll (Collagen I; fibrous powder from bovine tendon, Advanced Biomatrix, USA) were dissolved in 5 mM acetic acid by continuous stirring for 24 h. Blending this with the same amount of 1 % NaOH yielded a 2 wt% Coll solution. For hybrid scaffolds (1 wt% HA and 1 wt% Coll), 2 wt% HA and 2 wt% Coll precursor solutions were blended 1:1. In both compositions, 0.7 wt% ethylene glycol diglycidyl ether (EGDE) was added as chemical crosslinker. The resulting solutions were poured into cylindrical molds and frozen at -20°C for 6 days to allow cryogelation. The resulting microporous gels were thawed, subsequently swollen in water and washed with PBS (Phosphate Buffered Saline, PAN Biotech).

2.1.2. 3T3 fibroblast cells for monitoring ECM degradation and viability in 3D gels

After washing the gels, they were placed in 12-well plates, washed with DMEM (Dulbeco's Modified Eagles Medium, PAN Biotech), supplemented with 10 % FCS (Fetal calf serum, PAN Biotech) and immersed in DMEM/FCS. Cells were passaged according to a routine protocol and cultivated under standard conditions (37°C, 5 % CO_2, 90 % rel. humidity).

NIH-3T3 fibroblasts were transfected with LifeAct RFP using an electroporation protocol. In brief, the pellet was washed twice and resuspended in ice-cold electroporation buffer (consisting of 120 mM KCl, 10 mM K_2HPO_4/KH_2PO_4, pH 7.6, 2 mM $MgCl_2$, 25 mM HEPES pH 7.6 and 0,5 % Ficoll 400 in ddH_2O. The electroporation was performed in a 0.4 cm cuvette according to the experimental protocol (250 V/ 950 µF) with a BioRad elecroporator. The cells were recovered on ice and subsequently seeded in supplemented culture medium.

For seeding, cells were detached using 0.25 % trypsin/EDTA (ethylenediaminetetraacetic acid) in PBS and suspended in supplemented medium. Cells were seeded onto the gels at a density of 75 000 cells per gel (235 mm^3). Initially, they were allowed to migrate into the pores of the scaffold without additional medium for 30 min at 37°C. Later, 2 ml medium were added and the cells were cultivated for 8 days. All supernatant medium was exchanged every second day.

Live/dead assay was performed with non-transfected cells to avoid interference of the fluorescence signals. After 1, 4 and 8 days of cultivation, 0.5 µl Calcein (Thermo Fischer Scientific, 4 mM in DMSO (dimethyl sulfoxide) and 2 µl Ethidium homodimer (Thermo Fischer Scientific, 2 mM in DMSO/water) were added directly into the 2 ml nutrient medium in separate wells for each time point. Calcein and Ethidium homodimer were applied at a final concentration of 0.25 and 1 µl/ml medium, respectively. After incubation for 15 min, at least 5 laser scanning microscope (LSM; LSM 500, Zeiss) images were recorded during 15 min. In all images, living and dead cells were counted and the count was averaged for all images corresponding to one time-point. All experiments were done in triplicate. For each biological replicate, gels from a newly synthesized batch were used.

2.1.3. hMSC culture for monitoring ECM remodeling during differentiation in 2D and in 3D

Human bone marrow-derived MSCs (kindly provided by Prof. Dr. Karen Bieback, German Red Cross Blood Service Baden-Wuerttemberg/Hessen, Mannheim) were seeded in a density of

2000 cells/cm^2 on TPC and cultured in DMEM high glucose (Sigma-Aldrich) with 5 % human platelet lysate (PL; PL Bioscience, Aachen) and 2 U/ml heparin (PL Bioscience) under standard cell culture conditions (37°C, 5 % CO_2). Cells were subcultured at ~ 80 % confluency and passages 2 to 6 were used for the experiments. For seeding hMSCs into 3D scaffolds, cells were washed with PBS and detached using trypsin/EDTA solution (0.05/0.02 wt%, Sigma-Aldrich). After 5 min at 37°C, the trypsinization was stopped by addition of DMEM with 10 % FCS (Sigma-Aldrich). The cells were then centrifuged and re-suspended in DMEM with 5 % PL and 2 U/ml heparin. Finally, the highly concentrated cell suspensions were seeded onto 3D scaffolds (1 wt% HA / 1 wt% Coll) to final densities of 32x10^4 and 16x10^4 cells/118 mm^3 for adipogenic and osteogenic differentiation, respectively. After allowing for migration of the cells into the gels for 15 min at 37°C, the total amount of medium was adjusted with DMEM, supplemented with 5 % PL, 2 U/ml heparin and 100 U/ml penicillin and 100 µg/ml streptomycin (Sigma-Aldrich) to 500 µl/well.

2.1.4. Adipogenic and osteogenic differentiation of hMSCs

After the initial 24 h of cell cultivation, the medium was removed and replaced by 500 µl adipogenic induction medium (MSC Adipogenic Differentiation Medium 2, Promocell) with 100 U/ml penicillin and 100 µg/ml streptomycin (Sigma-Aldrich) to induce adipogenic differentiation. Osteogenic differentiation, hence, was induced by 500 µl osteogenic induction medium (MSC Osteogenic Differentiation Medium, Promocell) with 100 U/ml penicillin and 100 µg/ml streptomycin (Sigma-Aldrich) per well. Control samples with the respective cell count were further on cultured in DMEM with 5 % PL, 2 U/ml heparin and 100 U/ml penicillin and 100 µg/ml streptomycin (Sigma-Aldrich). For all conditions, the medium was changed twice per week and cells were cultured for 21 days.

2.1.5. HUVEC cell culture for monitoring ECM remodeling in 2D

HUVECs were isolated as described previously [67] after having obtained informed consent and transfected with a lentiviral vector to express dTomato. The cells were cultured using Endothelial Cell Growth Medium 2 (Promocell) supplemented with penicillin/streptomycin.

For MPT measurements HUVEC were seeded in 24-well plates (Nunc, Thermo Fischer Scientific) with a density of 7500 cells/cm^2. Every second day, medium was changed completely. For investigating ECM between the cells, cells were investigated by MPT at ~50% confluency.

For the protease inhibitor conditions, the medium was supplemented with 1 µl/ml or 5 µl/ml Halt protease inhibitor cocktail (Thermo Fischer Scientific). The control condition was kept in culture medium. For the high glucose condition, simulating high blood glucose in diabetes, the medium used for the whole cultivation, was supplemented with 100 mmol/l glucose, according to WHO's diagnostic criteria for diabetes $\geq$7.0 mmol/l fasting plasma glucose [68]. After 48h the culture medium was aspirated and replaced with PBS containing MPT particles.

2.2. Characterization of local viscoelastic matrix properties using MPT

2.2.1. MPT in general

The underlying principles and fluid mechanics of MPT microrheology have been described in detail [69,70]. In brief, the Brownian motion of inert colloidal probe particles embedded in a material is monitored. Thereby, quantitative information about the rheological properties of the surrounding fluid is obtained [71] based on a fundamental relationship between tracer mean square displacement (MSD) as a function of lag time τ and the complex shear modulus $G^*(\omega)$ as a function of the frequency. The Laplace transform of the particle MSD is related to the complex modulus G^* of the sample via a generalized Stokes-Einstein equation (GSE, general form, see Eq. (1)) [72,73]:

$$G^* = \frac{2k_BT}{3\ \pi\ a\ i\ \omega\Delta r^2(i\omega)} \tag{1}$$

a stands for the radius of the embedded beads, k_B for the Boltzmann constant and T for the temperature. This GSE relation is valid in 2D under the assumption that the material surrounding the tracer particles can be treated as an isotropic and homogeneous continuum, i.e. that the particle size is larger than the structural length scales of the probed material. Furthermore, tracer particle and fluid inertia need to be neglectable, which is appropriate here, since Reynolds number and Stokes number both are well below 1.

For 2D tracking of beads suspended in an ideal elastic material, Eq. (1) reduces to Eq. (2) [73,74]

$$G_0 = \frac{2k_BT}{3\ \pi a\Delta r^2(\tau)} \tag{2}$$

where G_0 stands for the frequency independent shear modulus of the material. As confirmed by the time independency of the MSDs (at τ = 0.1s), all materials investigated here, behave like elastic solids. As the collagen gels considered here are heterogeneous materials, MPT does not yield the true bulk modulus, thus G_0 is termed apparent modulus $G_{0,app}$ in the following.

In the first step of the MPT evaluation procedure, all particle trajectories are represented in a trajectory plot. Trajectories of freely diffusing particles cover a larger area compared to trajectories of elastically trapped particles, that are more restricted in their motion. Furthermore, areas in which no particles were present throughout the whole measurement can be identified.

Then from these trajectories, the coordinates of the particle centroids were transformed into MSD traces.

Time independent MSDs correspond to elastically trapped particles, whereas for freely diffusing particles, a linear increase over lag time τ is expected. Complex polymer materials often yield ensembles of MSDs including tracers of both limiting cases, and often also curved MSDs representing diffusion in a viscoelastic environment. Thus, the variation of obtained MSDs in one measurement provides insight into the heterogeneity of the material within the field of view (127 $\times$ 127 µm). In order to characterize the material heterogeneity often the Van Hove correlation function [75] is used and the non-Gaussian parameter α is calculated [76]. This parameter describes the deviation of the MSD values from a Gaussian distribution expected for an ideal homogeneous uniform sample (α = 0) at a fixed lag time τ. Real fluids with $\alpha \leq 1$ are considered homogeneous on the probed length scale typically ranging from 0.1 to 1 µm.

For image analysis, the software Image Processing System (Visiometrics iPS, Visiometrics GbR, Germany) was used and the calculation of MSDs and moduli was performed using a self-written Matlab code [73–76]. The evaluation routine is described in more detail in [62].

2.2.2. MPT in 3D scaffolds and 2D cell culture

For MPT in porous gels, the inverted fluorescence microscope (Axio Observer, Carl Zeiss, Germany, see Fig. 1A) was equipped with a high precision objective (Fluar 100x, N.A. 1.3, working distance 0.17 mm, Carl Zeiss). Images were recorded for at least 20s using a sCMOS camera Zyla X (Andor Technology, Ireland: 21.8 mm diagonal sensor size, 2160 $\times$ 2160 square pixels). We have also determined the so-called static error χ as described by Savin et al. [77]for our experimental setup. This quantity corresponds to the apparent random motion of particles due to the noise of the camera and digitization effects. It has been evaluated by fixing tracer particles on a substrate, and by performing measurements under

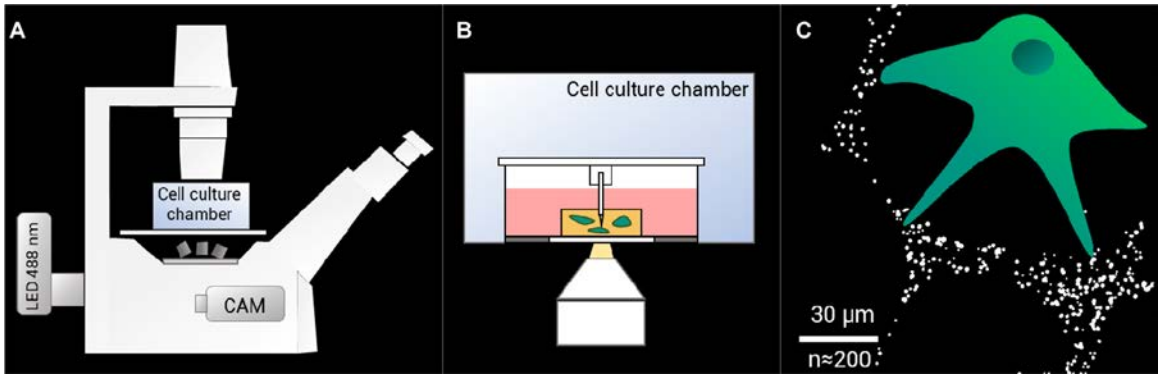

Fig. 1. Schematic of our Live Cell MPT setup used to monitor the change in ECM viscoelasticity in the surrounding of 3T3 fibroblasts cultured in porous 2 wt% Coll scaffolds: A) Sketch of the used experimental setup consisting of an inverted fluorescence microscope, equipped with a colored light source (LED), a high speed camera (CAM) and a high magnification objective. B) close-up of the cell-culture chamber, in which cell-laden gels are investigated in a glass-bottom petri dish. The needle avoids motion of the scaffold, while it is immersed in fluid. C) Resulting field of view showing a cell in the porous scaffold with tracer particles embedded in the pore walls.

similar noise and signal conditions as for the rest of the experiments. The static error for the experimental setup and tracer particles used here was χ ~10^{-4} µm^2 and defines the lower limit of accessible MSD.

Non-functionalized, surfactant stabilized polystyrene microspheres of diameter 0.2 µm (Bangs Laboratories, USA) were added together with EGDE during gel preparation [50] and the gels were placed in glass bottom petri dishes (Cell E\&G, \#GBD00004-200) or on conventional glass slides (Carl Roth, \#1) see Fig. 1B).

Fibroblasts and HUVECs were located by their actin cytoskeleton which showed red fluorescence after transfection with LifeAct RFP. For the localization of MSCs, a cell plasma membrane staining kit (orange fluorescence Cytopainter, Abcam) was used. This allowed us to localize the spatial expansion of the cells without fixation. In Fig. Fig. 1C, an exemplary field of view with a cell (scheme) and particles embedded in the surrounding pore walls of a hydrogel is shown. With our setup the thermal motion of tracer particles in the vicinity of cells located in a depth of about 20 µm within the porous scaffolds was investigated. The depth of focus was 0.3 µm according to the specifications of the objective given by the manufacturer, i.e. we essentially performed a 2D tracking.

In our so-called LiveCell MPT experiments (see Fig. 1), only tracer particles in the direct environment of single living cells (field of view 127 $\times$ 127 µm^2), well embedded in the scaffolds, were considered.

We used this setup for two different experiments:

(i) A series of discontinuous measurements was performed at room temperature. For each point of time and each condition, at least 6 sets, corresponding to 6 different locations in the scaffold, were recorded within 5 min operating time and analyzed subsequently. For each experiment, 3 biological replicates were investigated.

(ii) Continuous measurements were performed monitoring the same field of view/the same living cell at all time-points. The seeded scaffold was therefore kept in cell culture conditions using a cell culture chamber (Pecon CTI controller 3700). The measurement was started after adding the final amount of medium during the seeding protocol, the subsequent measurements were performed hourly for the first 8 hours after seeding. The shown values are thus single values determined in the surrounding of one and the same single cell.

In 2D cell cultures, MPT measurements were performed directly in the well plates, using a long distance objective (LD EC Epiplan neofluar 100 $\times$ 0.75 DIC, N.A. 0.75, working distance 4 mm, Carl Zeiss). To enhance the fluorescence signal, tracer particles with diameter 0.96 µm were used and these were added to the media 15 min prior to the measurement, yielding a final particle concentration of 0.017 wt%.

All measured values are shown as mean of 3 independent biological replicates with standard deviation Differences between groups were tested with one-way ANOVA (performed in Origin(Pro), Version 2019b, OriginLab Corporation, Northampton, USA) and considered significant if $p \leq 0.05$).

The section below summarizes the statistical analysis of the MPT experiments.

For gels with fibroblasts (section 3.1, Fig. 2C), MPT experiments were performed in triplicate and for each measurement, at least 6 sets of images corresponding to 6 different locations in the gel were considered. Results shown in Fig. 3 refer to a single MPT experiment for each point in time.

For gels including hMSC cells (section 3.2, Fig. 4A), all values are shown as mean of 3 independent biological replicates with standard deviation. For ECM secreted by HUVECs (section 3.3, Fig. 5C), averaged apparent moduli resulting from 2 biological replicates with 6 sets each, are shown as function of frequency. Error bars indicate standard deviation.

2.2.3. Rotational rheometry

The bulk viscoelastic properties of cell-laden gels and cell-free controls were characterized through their storage modulus G' and loss modulus G" as a function of frequency. Measurements were performed using a rotational rheometer (Physica MCR501, Anton Paar) with a plate-plate geometry (diameter 8 mm). Gap height was adjusted between 1 and 2 mm depending on the height of the samples, swollen in DMEM/FCS, to adjust the normal force to 0.15$\pm$0.05 N. For all conditions, frequency sweeps were performed in the linear regime at a stress amplitude of $\tau =$ 0.5 Pa, covering the frequency range of 0.1 to 10 rad/s. No evidence of wall slip was found in preliminary experiments performed at different gap heights. Modulus data provided below are a mean of two independent measurements.

2.3. Proof of hMSC differentiation by staining

2.3.1. Von Kossa staining

Osteogenic differentiation was visualized by von Kossa stain. Hereby, the phosphate ions in mineralic components, characteristic for the ECM in osteogenic differentiation, are precipitated with silver ions, so that hydroxyappatite and calciumphosphate depositions appear black.

After being cultured for 3 weeks, 2D cell cultures were fixed with 10 vol% formaldehyde (Applichem) for 15 min, subsequently washed with ddH_2O and stained with 5 wt% silver nitrate solution

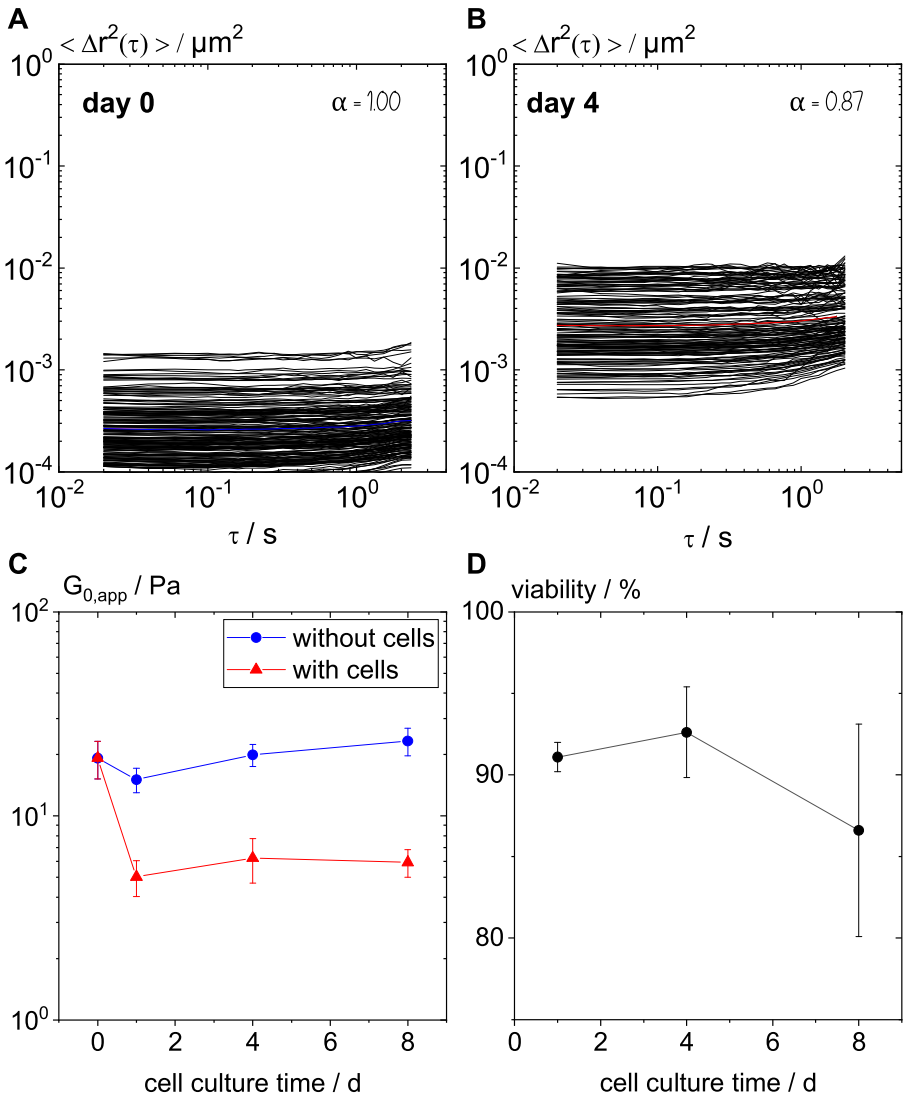

Fig. 2. Degradation of 1 wt% HA / 1 wt% Coll scaffolds by 3T3 cells: A) MSD plots and non-Gaussian parameter α, resulting from MPT video sequences, recorded directly after seeding (day 0) B) and after 4 days of cell culture. C) Plateau modulus $G_{0,app}$ over cell culture time for scaffolds with and without cells, determined from at least 6 independent measurements per condition and D) Cell viability, measured from 10 images per time point.

(Merck, Darmstadt) for 15 min. Thereafter, samples were washed with ddH_2O and incubated in 1 wt% Pyrogallol (Merck) in dark for 2 min. The staining was then washed with ddH_2O and fixed with 5 wt% sodium thiosulfate for 5 min followed by a last washing step with ddH_2O. Optical images were obtained using an inverse fluorescence microscope (Axio Vert A1, Carl Zeiss, Oberkochen) and a camera (Axiocam Cc1 60N-C1"1.0x camera, Carl Zeiss).

2.3.2. Oil Red staining

For the visualization of adipogenic differentiation in 2D after 3 weeks of culture, fat vacuoles were stained by Oil Red. After cell fixation in 10 vol% formaldehyde and washing with ddH_2O, 60 vol% isopropanol (VWR) were added and incubated for 2 min. Oil Red O (Sigma-Aldrich) working solution was prepared from a 0.3 %(wt/vol) Oil Red stock in isopropanol by diluting this 3:2 with ddH_2O. The final concentration was 0.18 % (wt/vol) and remaining solids were removed by centrifugation. 250 µl of the staining solution were added per well and incubated for 5 min. Subsequently, the samples were washed with tap water, until clear supernatant was obtained. Cell nuclei were stained purple with hematoxylin solution, Harris modified (Sigma-Aldrich) for 2 min. After a final washing with tap water, images were taken using an inverted fluorescence microscope (Axio Vert A1, Carl Zeiss, Oberkochen) and a camera (Axiocam Cc1 60N-C1"1.0x camera, Carl Zeiss).

3. Results and discussion

3.1. Continuous monitoring of matrix degradation by fibroblasts

Fibroblasts are known to remodel their environment extensively by secreting proteinases that degrade collagen-rich matrix structures. We used for the first time MPT to characterize the effect of fibroblast growth on the local viscoelastic properties of a HA / Coll scaffold in the direct cell surrounding. In a first approach, this effect was monitored during 8 days of cell culture by investigation of the scaffolds local mechanical properties with MPT experiments directly after cell seeding and after 1, 4 and 8 days of cell cultivation. Per time point, 9 experiments were performed, i.e. 9 fields of view were investigated. Thus, the mechanical properties were characterized on a length scale of one field of view (127 × 127 µm for the setup shown in Fig. 1) and the $G_{0,app}$ values for all cells in a cell population were averaged.

Fig. 2A and B show the variation of MSDs as a function of lag time for tracer particles (diameter = 0.19 µm), dispersed in the

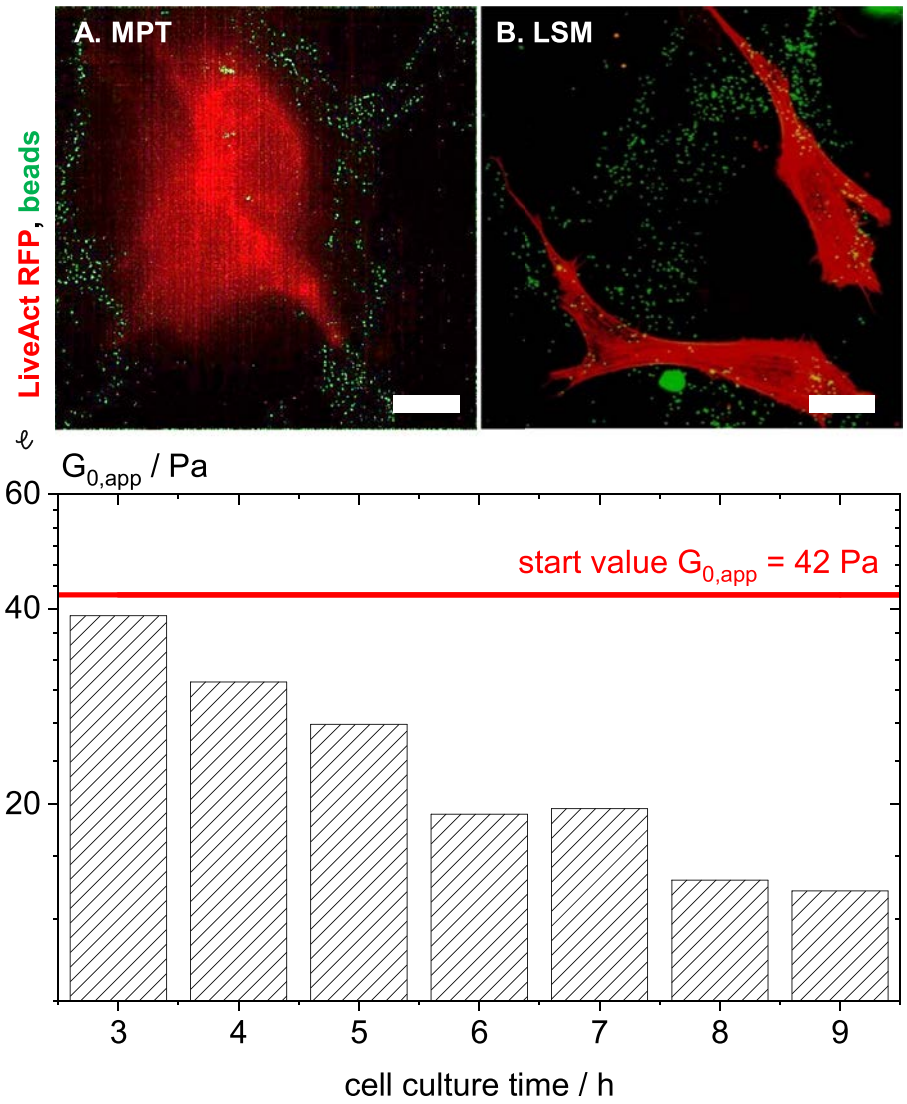

Fig. 3. Continuous LiveCell MPT: A) Microscope image, taken with the inverted fluorescence microscope (555 and 488 nm colored LED) and high speed camera of the MPT setup, showing MPT tracers distributed in the 2 wt% Coll scaffold matrix (green) and the actin cytoskeleton of the imaged 3T3 cell (transfected with LifeAct RFP, red) and B) same scaffold visualized using LSM and C) time evolution of $G_{0,app}$ in the direct cell surrounding of an individual living 3T3 cell.

matrix of 1wt% HA / 1 wt% Coll cryogel scaffolds directly after cell seeding and after 4 days of culture, respectively. In both cases, all MSD traces exhibit almost no time dependence in the investigated lag times (τ in s) and their absolute values show a narrow distribution within 1.5 decades. Consequently, the non-Gaussian parameter α is $\leq$1. These results indicate that the tracer particles are at all time-points (culture time in days) trapped elastically in a homogeneous, gel-like network. However, the mean MSD (shown as colored line in Fig. 2A and B) increased from $\approx$2.5x 10^{-5} directly after seeding to $\approx$3x10^{-3} μm^2 after 4 days of cell cultivation. This indicates a reduction in matrix stiffness, corresponding to a decrease of the elastic plateau modulus.

Fig. 2C shows the evolution of the matrix stiffness over the entire 8 days of cell cultivation. The elastic plateau values obtained from MPT measurements after 0, 1, 4 and 8 days with (red) and without cells (blue) are shown. In the cell-laden scaffolds, a strong decrease of the scaffolds' stiffness was observed within the first day. $G_{0,app}$ decreased from 19$\pm$4 to 5$\pm$1 Pa (see Fig. 2C) as calculated from the average value of the resolved lines in Fig. 2A and B according to Eq. (2). This decrease in matrix stiffness in the direct cell surrounding results presumably from the fibroblasts remodeling the ECM by upregulating proteinase activity to design matrix elasticity according to their current needs [78].

A disturbing effect of cells contractility on MPT measurements of ECM mechanical properties can be excluded here since similar elasticity values were obtained for scaffolds with and without cells (see Fig. 2C, cell culture time 0 h).

During the following days, $G_{0,app}$ remained constant at a value of 6$\pm$2 Pa till day 8. In contrast, the elasticity of cell-free scaffolds was almost constant during the entire experiment with $G_{0,app}$ ranging between 18 and 22 Pa which indicates that no degradation took place. This confirms furthermore, that the decrease in matrix stiffness is not related to any chemical modification or enzymatic degradation due to the reaction with cell culture media components, but caused by the metabolic actions of the cultured cells.

This change in local viscoelasticity near the embedded cells does not show up in bulk shear modulus measurements. $G_{0,bulk}$ ($\approx$ 21 kPa) remains constant for the entire duration of the experiments and no difference between gels with or without cells can be detected. It should be noticed that the bulk modulus $G_{0,bulk}$ is about three orders of magnitude higher than $G_{0,app}$. This was

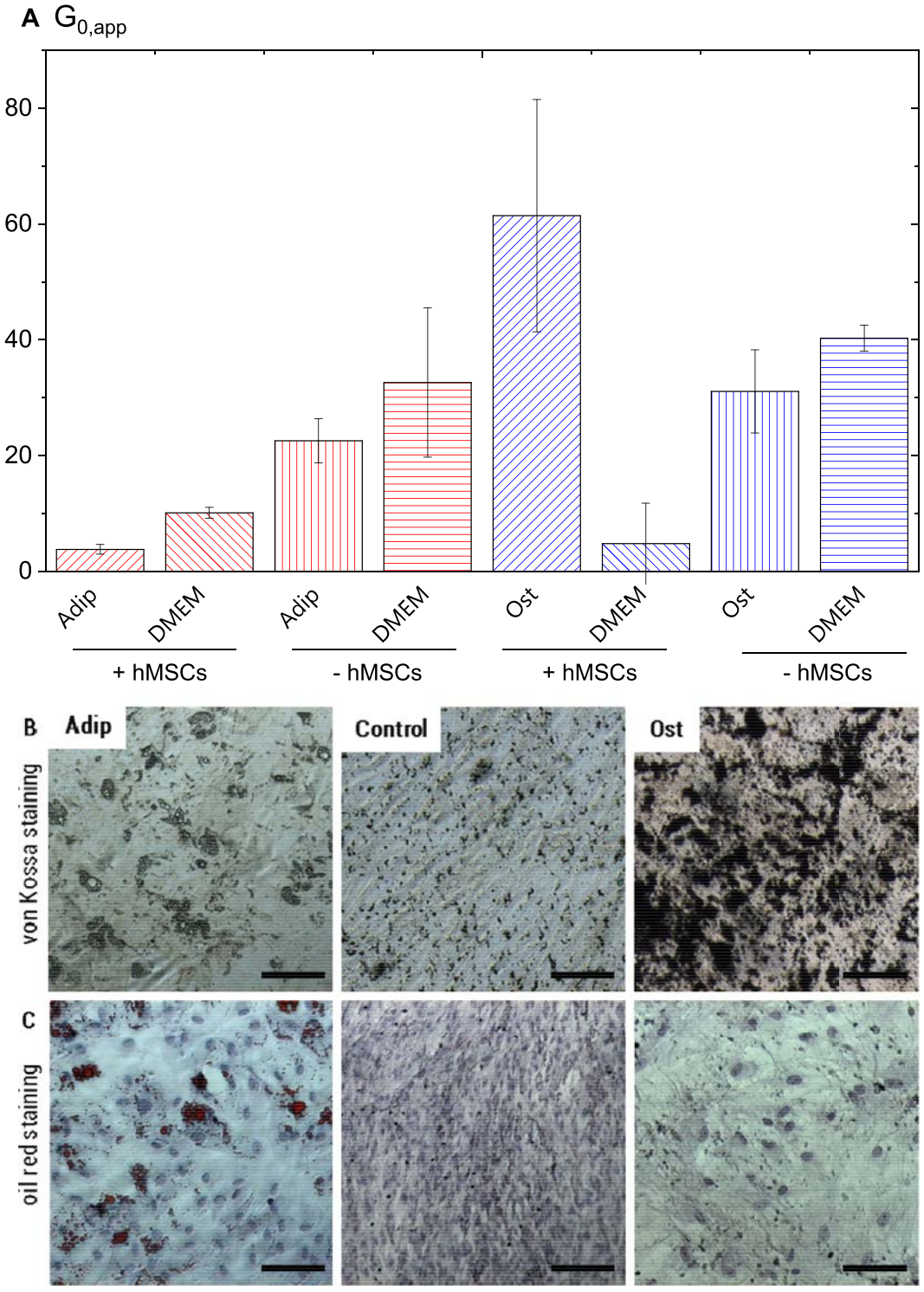

Fig. 4. MPT as versatile tool to monitor matrix mechanics during cell differentiation in 3D scaffolds: A) $G_{0,app}$ in the direct cell environment, measured for MSCs cultured for 21 days in adipogenic differentiation medium (Adip), osteogenic differentiation medium (Ost) and respective cell densities cultivated in control medium (DMEM). Corresponding data for empty gels (- hMSCs) are shown for comparison and cell-laden scaffolds are labeled accordingly (+ hMSCs). All measured values are shown as mean of 3 independent biological replicates with standard deviation. B) Visualization of hydroxyappatite formation in the ECM during osteogenic differentiation by von Kossa staining (black) of adipogenic, control and osteogenic condition and C) Visualization of oil vesicles (red) by Oil Red staining of adipogenic, control and osteogenic condition. Nuclei are stained in blue. Images are obtained in 2D; all scale bars represent 100 µm.

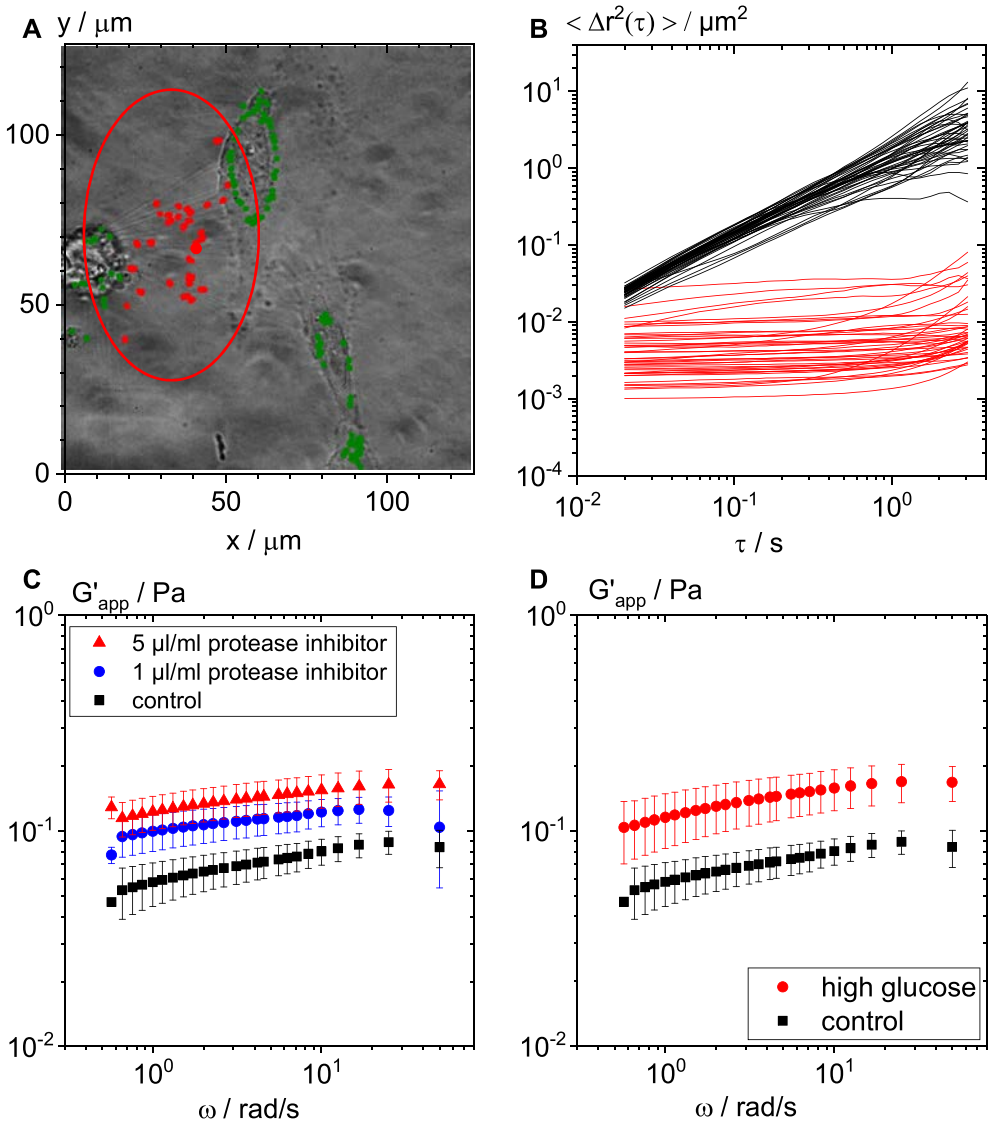

Fig. 5. MPT allows for characterization of newly secreted ECM in scaffold-free 2D cell culture of HUVECs: A) Light microscopy image showing 3 cells and thin fibers connecting them, in overlay with trajectories of 0.2 µm MPT tracers, sensing elastic environment (slope of the MSD < 0.5) used for characterization of the inter-cellular network / ECM (red). Those that were excluded from the analysis, because they might be sticking to the cell surface are shown in green. B) resulting MSD plots for a typical experiment with the cellular layer in PBS showing the two populations for the elastic ECM (red) and viscous PBS (black). C) Effect of protease inhibitor on the ECM elasticity. Control (black) is compared to two inhibitor concentrations, 1 µl/ml (blue) and 5 µ/ml (red). D) Comparison of the elasticity of secreted ECM under high glucose (100 mmol/l glucose) and control (5.6 mmol/l glucose) conditions.

observed for various other biomaterials [51,79]. For the scaffolds used here, it is discussed in [50] in more detail.

MPT resolves the mechanical properties locally on a length scale that is relevant for cells' mechanosensing [23,33]}. The viability of the fibroblasts (see Fig. 2D) is >85 % during the whole experiment, i.e. the observed changes in the matrix elasticity are related to the metabolic activity of a healthy population of fibroblasts. A high number of apoptotic cells might cause additional weakening of the matrix due to secretion of large amounts of intracellular enzymes, but this is not the case here.

As we have seen in Fig. 2C, the degradation of the scaffold mainly takes place within the first day. This important initial period of time was further investigated in a second approach, using a novel MPT setup including a cell-culture chamber (see Fig. 1). Using this, we were able to monitor the matrix elasticity in the direct surrounding of one single cell during the first 9 h after seeding. Fig. 3A shows the overlay of the fluorescence signal resulting from the actin cytoskeleton (red) and from the tracer particles embedded in the surrounding pore walls (green). The images were obtained by the using the inverted fluorescence microscope of the MPT setup, where background fluorescence and blur, especially in the red channel, cause large shadows and the resolution in depth is limited. For verifying characteristic, healthy fibroblast morphology, a 3D image obtained from LSM is shown in Fig. 3B. In MPT experiments, the red fluorescent cytoskeleton still helps to localize the cells in the 3D scaffold. LSM is, however, not suitable for MPT experiments, due to the long scanning times. For evaluating mechanical properties, the Brownian motion of the tracer particles is in focus and therefore, after recording the 555 nm signal initially, MPT videos for data evaluation are taken with the 488 nm light source only, to reduce noise. Between the single video recordings, cells were kept in the dark and only for the measurement, the light source was switched on.

Fig. Fig. 3C shows the gradual reduction of matrix stiffness in the direct environment of the investigated single cell through the variation of the plateau modulus $G_{0,app}$ Starting from 42 Pa,

measured immediately after seeding, a continuous decrease in $G_{0,app}$ is observed within the following 9 h, yielding a final value of 15 Pa. This ratio of final to initial modulus is in good accordance with the averaged results obtained for a whole population of fibroblasts, shown in Fig. 2. Consequently, this single cell, as well as all other cells considered in the aforementioned experiments, continuously decreased the elasticity of the scaffold in their direct surrounding, most likely by upregulating MMP activity [80]. These enzymes are known to cleave peptide bonds in e.g. collagen structures. *In vivo*, the enzymatic activity of MMPs underlies a complex regulation cycle, including the availability of MMP inhibitors, which helps the cells to maintain the mechanical properties of their ECM [80]. In 3D scaffolds, however, cells need to remodel the scaffolds provided to them. Most likely, the observed continuous decrease is driven by the discrepancy between the stiff scaffolds provided and the desired softer ECM the cells try to achieve by degrading the artificial ECM. Followingly, upregulating MMP expression in cells seeded on stiffer scaffolds is already shown in other studies [81,82] and could be one explaining mechanism to adjust the given scaffold by the cells in our study.

Processes like this can be elucidated in more detail and on shorter time scales, referring to one single cell by combining the MPT setup with a cell culture chamber.

3.2. ECM mechanics after adipogenic and osteogenic differentiation in 3D

In vivo, MSCs differentiate according to current needs, e.g. responding to exercise or regenerating connective tissue in order to compensate lacking cells [83]. During differentiation either into the osteoblast or the adipocyte lineage, their phenotype is completely changed, including metabolic function and the ability to build up completely different tissues [83,84]. The mechanical properties of such tissues depend on the stiffness of the cells and, especially in ECM rich tissues, on the mechanical properties of the ECM connecting the cells [33,85].

Using adipogenic and osteogenic differentiation inducing media in 3D hMSC cultures based on 1 wt% HA / 1 wt% Coll scaffolds, we studied the mechanical properties in the cells' environment after terminal differentiation into adipocytes and osteoblasts, respectively. In Fig. Fig. 4, the local plateau modulus, obtained from MPT measurements in the scaffold-network, is shown for cell-laden and cell-free samples.

After 21 days of cell culture, in the adipogenic differentiation medium (Adip), a difference in $G_{0,app}$ of $\approx$19 Pa was found between cell-laden (3.8$\pm$0.8 Pa) and cell-free scaffolds (22$\pm$4 Pa). The same initial cell count in MSC maintenance medium (DMEM, control) yielded a similar decrease of $\approx$22 Pa in the cell-laden scaffold (10.1$\pm$0.9 Pa) compared to the cell-free control (32$\pm$13 Pa). Under both conditions, the scaffold elasticity is reduced by the cells, but it is worth considering the difference in cell numbers. Continuous proliferation in DMEM should result in much higher cell numbers compared to low proliferation rates during adipogenic differentiation. Thus, the decrease of $G_{0,app}$ in adipogenic condition is caused by a presumably much smaller number of cells than in the control condition, so that the scaffold-softening effect per cell can be considered to be stronger during adipogenic differentiation.

In the case of osteogenic differentiation (Ost), a significant increase of $\approx$ 30 Pa in $G_{0,app}$ is observed for the cell-laden scaffold (61$\pm$20 Pa) compared to the cell-free counterpart (31$\pm$7 Pa). In contrast, in DMEM, a decrease by almost a factor of 10 was found when comparing cell-free (40$\pm$2 Pa) to cell-laden scaffolds (5$\pm$5 Pa).

As commonly assumed, the osteoblasts that result from the osteogenic differentiation do not only secrete collagen and other ECM compounds, but also contribute to the calcification of the existing ECM [57,58].

Our tracer particles are embedded in the scaffold matrix, so that their motion is more restricted by the stiffening network. Thus, higher values for $G_{0,app}$ are obtained, showing MPT's unique capability to quantify the differences in matrix elasticity, which result from differentiation here.

Comparing adipogenic and osteogenic conditions, we see a total difference of about 60 Pa in the local elasticity of both cell laden scaffolds, reflecting the extreme difference in mechanical properties in the corresponding tissue types *in vivo* - bone and adipose tissue, whose tissue E modulus differ in more than four orders of magnitude [86].

To proof that the measured effects on local matrix elasticity were derived from successful differentiation of hMSCs, we employed von Kossa and Oil Red staining protocols. Von Kossa (see Fig. 4B) makes mineralization in the ECM visible, large mineralized areas are clearly visible in the osteogenic induced sample (right), whereas in control (middle) and adipogenic (left) condition, only some unspecific grey shades occurred. Oil Red (see Fig. 4C) stains fat vacuoles in adipocytes. In adipogenic induced differentiation (first row), lots of fat vacuoles are seen in red, whereas in control (middle) and osteogenic (right) condition, only purple nuclei are visible.

To summarize, the induced differentiation was successful and the specific metabolic activity of osteoblasts and adipocytes resulted in a measurable difference in local ECM elasticity.

3.3. ECM mechanics in 2D

Seeded on conventional TCP (tissue culture plastic) without any scaffold, cells live in ECM that is exclusively secreted by themselves. This ECM is supposed to match their actual needs and is thus constantly remodeled by secretion of additional matrix components and degrading enzymes [80]. However, the total amount of newly secreted material in such a scaffold-free approach is much less than the amount of synthetic material provided in scaffold-based systems. Furthermore, the material is located on TCP and cannot be moved to glass slides without damaging it. Consequently, the use of a long distance objective is required and still, resolution and fluorescence intensity are reduced, compared to measurements on glass slides. Thus, the minimum particle size allowing for reliable tracking is 1 µm. Additionally, the natural ECM cannot be doped with particles during fabrication, so that for MPT, the particles need to be added later on. Thus, such 2D experiments work by adding tracer particles to the nutrient media surrounding a 2D cell layer after a few minutes waiting time some tracers are entrapped in the network built around the cells.

As this entrapment happens randomly, always two populations of tracer particles are found in such MPT experiments. Some particles are trapped in the newly secreted network (shown in red in Fig. 5A and B) and sense the local elasticity of the ECM. The other fraction continues to diffuse freely, sensing the viscosity of the solvent/media (shown in black in Fig. 5B). The viscosity values calculated from these MSDs agree very well with the data for pure PBS.

For the characterization of the mechanical properties of the ECM we use only the elastically trapped fraction of tracer particles and corresponding data is further processed to eliminate particles, that are sticking to cellular surfaces (shown in green), because we aimed at characterizing the ECM and not the mechanical properties of cells or their membranes. We use the generalized Stoke-Einstein equation (GSE, Eq. (1)) to calculate the complex shear modulus $G^*(\omega) = G' + iG''$. We do not know, whether the probed material is homogeneous and in thermal equilibrium, and accordingly we are not sure whether Eq. (1) is fulfilled here. Thus we have to treat the

calculated moduli as apparent values. Nevertheless, their variation indicates changes in the viscoelastic properties of the ECM.

For calculation of local apparent moduli, corresponding data is further processed to eliminate particles, that are sticking to cellular surfaces (shown in green), because we aimed at characterizing the ECM and not the mechanical properties of cells or their membranes.

Averaged apparent moduli resulting from 6 independent sets, measured in HUVEC cultures, are shown as function of frequency in Fig. 5C (black curve). Here we also show the effect of the concentration of additionally supplemented Halt protease inhibitor cocktail. This inhibitor cocktail is supposed to down-regulate the activity of the MMPs secreted by the cells during remodeling. The resulting matrix elasticity is shown in red (5 µl/ml inhibitor) and blue (1 µl/ml inhibitor) and compared to the control without inhibitor. In all cases, G' is essentially frequency independent. This indicates a gel-like behavior of the ECM, independent of the inhibitor concentration. However, the absolute values of $G_{0,app}$ (taken at at ω= 10 rad/s) increased significantly with increasing inhibitor concentration from 0.08±0.01 (no inhibitor) to 0.12±0.02 Pa (5 µl/ml). This proves the high sensitivity of MPT in the low elasticity range and is in good agreement with the reduced matrix degradation activity expected for high inhibitor concentration.

One potential application for studying mechanical properties of ECM is tissue reorganization associated with diabetes. Diabetes mellitus is characterized by a chronic hyperglycemia due to severe insulin resistance and/or insufficiency. Up to date there are various ECM modifications which are assumed to be involved in the pathomechanisms of diabetic complications. The most prominent mechanism is the formation of Advanced glycation endproducts (AGE), which are formed by non-enzymatic glycation of proteins [87,88]. The effect of AGE ranges from inflammatory activation [89] and modification of cellular migration [90] to alteration of mechanical properties of ECM caused by crosslinking of ECM molecules [91]. Collagen is one prominent ECM protein which is affected by the formation of abnormal, stable intermolecular crosslinks in a hyperglycemic context [92–94].

Another important mechanism is altered MMP/TIMP related ECM remodeling [95] as a cellular response in a diabetic environment.

The mechanical alteration in glycated matrix components alone [91] as well as changes of cell stiffness were investigated using AFM and MPT after endocytosis of tracer particles, respectively [96].

Especially vascular endothelial cells are exposed in first order to an elevated blood glucose level and it has been reported that hyperglycemia induces a complex dysfunction of endothelial cells [97,98] with the consequence of diverse micro- and macrovascular pathologies of diabetes [99–101].

Thus, we studied local elasticity of the ECM at very high glucose concentrations. For 100 mmol/l glucose, we found $G_{0,app}$ = 0.15±0.03 Pa, which is almost twice the value obtained under normal conditions (0.08±0.01 Pa, both measured at 10 rad/s). This alteration is presumably more related to osmosis and densification of the gel due to reduced water activity or chemical modification of the ECM by glucose itself (protein glycation), than related to alterations in cell metabolism.

4. Conclusion

Multiple particle tracking microrheology was successfully used to monitor the matrix remodeling of single fibroblast cells in 3D scaffolds continuously. During the first 9 h after seeding, a monotonic decrease in $G_{0,app}$ from 42 to 15 Pa was observed for a single cell and after 24 h, 5±1 Pa were measured in the discontinuous experiment averaging over multiple cells per time point. In contrast, no effect of growing cells showed up in conventional bulk shear experiments.

Furthermore, we characterized the ECM elasticity in hMSC cultures, where adipogenic and osteogenic differentiation was induced using specific differentiation media. We were able to prove that the osteogenic differentiation leads to a significant increase in local elastic modulus $G_{0,app}$ to ≈60 Pa of the HA / Coll based scaffolds with initial $G_{0,app}$ ≈30 Pa. This is related to the densification of the matrix by additional secretion of ECM components and the mineralization of the ECM during osteogenesis. In contrast, during adipogenic differentiation, the homoeostasis is shifted towards softer ECM and $G_{0,app}$ is consequently decreased significantly to ≈5 Pa.

Finally, we studied the secretion of new ECM in a scaffold-free 2D HUVEC culture with different concentrations of Halt protease inhibitor cocktail. Increased inhibitor concentration showed the expected increase of ECM elasticity from $G_{0,app}$ = 0.08±0.01 Pa for control condition to 0.12±0.02 Pa for the highest inhibitor concentration. Upon cultivation in high glucose concentration, a twofold increase in $G_{0,app}$ compared to the control was observed. The resolution of our setup can consequently be considered sufficient to characterize the remodeling of even very soft ECM in 2D.

The techniques shown here and their combination provide great potential for studying cell-matrix interactions and their continuous effect on matrix elasticity in 2D cultures and in near-natural 3D scaffolds. Providing deeper insight in the remodeling of artificial ECM substitutes can support the design of biomaterials with appropriate properties for cell culture. Furthermore, having a tool to investigate ECM elasticity can help us to understand diseases and perhaps unravel pathways for potential therapies modulating ECM mechanics.

Declaration of Competing Interest

The authors declare that they have no known competing financial interests or personal relationships that could have appeared to influence the work reported in this paper.

Acknowledgements

ALH, AR and CLT have received funding from the European Research Council (ERC) under the European Union's Horizon 2020 research and innovation program (grant agreement No 757490) and from the BMBF NanoMatFutur program (FKZ 13N12968).

MB and SB acknowledge support by the Helmholtz Association via the program "BioInterfaces in Technology and Medicine" (BIFTM); the Deutsche Forschungsgemeinschaft (DFG, German Research Foundation) under Germany's Excellence Strategy – 2082/1 – 390761711, Cluster of Excellence "3D Matter Made to Order" (3DMM2O) and by the Carl Zeiss Foundation.

Julian Gebauer acknowledges support by the International Research Training Group 1874/2 DIAMICOM and the Deutsche Diabetes Gesellschaft.

References

[1] J.A. Eble, S. Niland, The extracellular matrix in tumor progression and metastasis, Clin. Exp. Metastasis 36 (2019) 171–198.
[2] M.G. Haugh, The development of novel scaffolds for tissue engineering with a range of structural and mechanical properties, Doctoral Thesis, Trinity College Dublin (2009).
[3] H.-D. Hwang, H.-J. Cho, P. Balakrishnan, C.-W. Chung, I.-S. Yoon, Y.-K. Oh, Y. Byun, D.-D. Kim, Cross-linked hyaluronic acid-based flexible cell delivery system: application for chondrogenic differentiation, Colloids Surf. B Biointerfaces 91 (2012) 106–113.
[4] A. Tripathi, T. Vishnoi, D. Singh, A. Kumar, Modulated crosslinking of macroporous polymeric cryogel affects in vitro cell adhesion and growth, Macromol. Biosci 13 (2013) 838–850.
[5] I. Schoen, B.L. Pruitt, V. Vogel, The Yin-Yang of Rigidity Sensing: How Forces and Mechanical Properties Regulate the Cellular Response to Materials, Annu. Rev. Mater. Res. 43 (2013) 589–618.

[6] C. Lee-Thedieck, N. Rauch, R. Fiammengo, G. Klein, J.P. Spatz, Impact of substrate elasticity on human hematopoietic stem and progenitor cell adhesion and motility, Journal of Cell Science 125 (2012) 3765–3775.

[7] A.J. Engler, S. Sen, H.L. Sweeney, D.E. Discher, Matrix elasticity directs stem cell lineage specification, Cell 126 (2006) 677–689.

[8] A.J. Engler, M.A. Griffin, S. Sen, C.G. Bonnemann, H.L. Sweeney, D.E. Discher, Myotubes differentiate optimally on substrates with tissue-like stiffness: pathological implications for soft or stiff microenvironments, J. Cell Biology 166 (2004) 877–887.

[9] R.A. Marklein, J.A. Burdick, Controlling stem cell fate with material design, Advanced Materials 22 (2010) 175–189.

[10] B.D. Cosgrove, K.L. Mui, T.P. Driscoll, S.R. Caliari, K.D. Mehta, R.K. Assoian, J.A. Burdick, R.L. Mauck, N-cadherin adhesive interactions modulate matrix mechanosensing and fate commitment of mesenchymal stem cells, Nat. Mater. 15 (2016) 1297–1306.

[11] J.R. Staunton, W.Y. So, C.D. Paul, K. Tanner, High-frequency microrheology in 3D reveals mismatch between cytoskeletal and extracellular matrix mechanics, Proc. Natl. Acad. Sci. U. S. A. 116 (2019) 14448–14455.

[12] S. Bhat, A. Tripathi, A. Kumar, Supermacroprous chitosan-agarose-gelatin cryogels: in vitro characterization and in vivo assessment for cartilage tissue engineering, J. R. Soc. Interface 8 (2011) 540–554.

[13] K.-H. Chang, H.-T. Liao, J.-P. Chen, Preparation and characterization of gelatin/hyaluronic acid cryogels for adipose tissue engineering: In vitro and in vivo studies, Acta Biomaterialia 9 (2013) 9012–9026.

[14] M.N. Collins, C. Birkinshaw, Morphology of crosslinked hyaluronic acid porous hydrogels, J. Appl. Polym. Sci. 120 (2011) 1040–1049.

[15] S.-L. Loo, W.B. Krantz, T.-T. Lim, A.G. Fane, X. Hu, Design and synthesis of ice-templated PSA cryogels for water purification: Towards tailored morphology and properties, Soft Matter 9 (2013) 224–234.

[16] B.A. Roeder, K. Kokini, J.E. Sturgis, J.P. Robinson, S.L. Voytik-Harbin, Tensile Mechanical Properties of Three-Dimensional Type I Collagen Extracellular Matrices With Varied Microstructure, J. Biomech. Eng. 124 (2002) 214.

[17] M. Ahearne, Introduction to cell-hydrogel mechanosensing, Interface Focus 4 (2014) 20130038.

[18] A. Sharma, S. Bhat, V. Nayak, A. Kumar, Efficacy of supermacroporous poly(ethylene glycol)-gelatin cryogel matrix for soft tissue engineering applications, Mater. Sci. Eng. C Mater. Biol. Appl. 47 (2015) 298–312.

[19] S. Bhat, A. Kumar, Cell proliferation on three-dimensional chitosan-agarose-gelatin cryogel scaffolds for tissue engineering applications, J. Biosci. Bioeng. 114 (2012) 663–670.

[20] D. Berillo, B. Mattiasson, I.Y. Galaev, H. Kirsebom, Formation of macroporous self-assembled hydrogels through cryogelation of Fmoc-Phe-Phe, J. Colloid Interface Sci 368 (2012) 226–230.

[21] D. Singh, Proliferation of Myoblast Skeletal Cells on Three-Dimensional Supermacroporous Cryogels, Int. J. Biol. Sci. (2010) 371–381.

[22] J.R. Tse, A.J. Engler, Preparation of hydrogel substrates with tunable mechanical properties, Curr. Protoc. Cell Biol. 47 (2010) 10–16.

[23] N.D. Evans, E. Gentleman, The role of material structure and mechanical properties in cell–matrix interactions, J. Mater. Chem. B 2 (2014) 2345.

[24] K.A. Marx, T. Zhou, A. Montrone, D. McIntosh, S.J. Braunhut, Quartz crystal microbalance biosensor study of endothelial cells and their extracellular matrix following cell removal: Evidence for transient cellular stress and viscoelastic changes during detachment and the elastic behavior of the pure matrix, Anal. Biochem 343 (2005) 23–34.

[25] D.M. Ebenstein, L.A. Pruitt, Nanoindentation of soft hydrated materials for application to vascular tissues, J. Biomed. Mater. Res. A 69 (2004) 222–232.

[26] J.D. Kaufman, G.J. Miller, E.F. Morgan, C.M. Klapperich, Time-dependent mechanical characterization of poly(2-hydroxyethyl methacrylate) hydrogels using nanoindentation and unconfined compression, J. Mater. Res. 23 (2008) 1472–1481.

[27] T. Kuboki, W. Chen, S. Kidoaki, Time-dependent migratory behaviors in the long-term studies of fibroblast durotaxis on a hydrogel substrate fabricated with a soft band, Langmuir 30 (2014) 6187–6196.

[28] X.-Z. Zhang, Y.-Y. Yang, T.-S. Chung, K.-X. Ma, Preparation and Characterization of Fast Response Macroporous Poly(N -isopropylacrylamide) Hydrogels, Langmuir 17 (2001) 6094–6099.

[29] M.P.E. Wenger, L. Bozec, M.A. Horton, P. Mesquida, Mechanical properties of collagen fibrils, Biophysical Journal 93 (2007) 1255–1263.

[30] C.T. McKee, J.A. Last, P. Russell, C.J. Murphy, Indentation versus tensile measurements of Young's modulus for soft biological tissues, Tissue Eng. Part B Rev. 17 (2011) 155–164.

[31] A. Malandrino, M. Mak, R.D. Kamm, E. Moeendarbary, Complex mechanics of the heterogeneous extracellular matrix in cancer, Extreme Mech. Lett. 21 (2018) 25–34.

[32] P.K.V. Babu, C. Rianna, U. Mirastschijski, M. Radmacher, Nano-mechanical mapping of interdependent cell and ECM mechanics by AFM force spectroscopy, Sci. Rep. 9 (2019) 1–19.

[33] L.R. Smith, S. Cho, D.E. Discher, Stem cell differentiation is regulated by extracellular matrix mechanics, Physiology 33 (2018) 16–25.

[34] K. Tanner, High Frequency Active Microrheology Reveals Mismatch in 3D Tumor Intracellular and Extracellular Matrix Viscoelasticity, Biophysical Journal 116 (2019) 8a.

[35] B.A. Juliar, M.T. Keating, Y.P. Kong, E.L. Botvinick, A.J. Putnam, Sprouting angiogenesis induces significant mechanical heterogeneities and ECM stiffening across length scales in fibrin hydrogels, Biomaterials 162 (2018) 99–108.

[36] M. Keating, A. Kurup, M. Alvarez-Elizondo, A.J. Levine, E. Botvinick, Spatial distributions of pericellular stiffness in natural extracellular matrices are dependent on cell-mediated proteolysis and contractility, Acta Biomaterialia 57 (2017) 304–312.

[37] D. Mizuno, C. Tardin, C.F. Schmidt, F.C. MacKintosh, Nonequilibrium mechanics of active cytoskeletal networks, Science 315 (2007) 370–373.

[38] M.A. Kotlarchyk, E.L. Botvinick, A.J. Putnam, Characterization of hydrogel microstructure using laser tweezers particle tracking and confocal reflection imaging, J. Phys. Condens. Matter 22 (2010) 194121.

[39] H. Li, J.M. Mattson, Y. Zhang, Integrating structural heterogeneity, fiber orientation, and recruitment in multiscale ECM mechanics, J. Mech. Behav. Biomed. Mater. 92 (2019) 1–10.

[40] Y.L. Han, P. Ronceray, G. Xu, A. Malandrino, R.D. Kamm, M. Lenz, C.P. Broedersz, M. Guo, Cell contraction induces long-ranged stress stiffening in the extracellular matrix, PNAS 115 (2018) 4075–4080.

[41] C. Gambini, B. Abou, A. Ponton, A.J.M. Cornelissen, Micro- and macrorheology of jellyfish extracellular matrix, Biophysical Journal 102 (2012) 1–9.

[42] N. Nijenhuis, D. Mizuno, J.A.E. Spaan, C.F. Schmidt, High-resolution microrheology in the pericellular matrix of prostate cancer cells, J. R. Soc. Interface 9 (2012) 1733–1744.

[43] Y. Tseng, T.P. Kole, D. Wirtz, Micromechanical Mapping of Live Cells by Multiple-Particle-Tracking Microrheology, Biophysical Journal 83 (2002) 3162–3176.

[44] J.C. Crocker, B.D. Hoffman, Multiple-Particle Tracking and Two-Point Microrheology in Cells, Methods in Cell Biology Cell Mechanics, Academic Press, 2007, pp. 141–178.

[45] Oosten, Anne S. G. van, M. Vahabi, A.J. Licup, A. Sharma, P.A. Galie, F.C. MacKintosh, P.A. Janmey, Uncoupling shear and uniaxial elastic moduli of semiflexible biopolymer networks: compression-softening and stretch-stiffening, srep 6 19270.

[46] D.P. Jones, W. Hanna, J.P. Celli, Mapping dynamic mechanical remodeling in 3D tumor models via particle tracking microrheology, Optical Elastography and Tissue Biomechanics II, SPIE, San Francisco, California, United States, 2015, p. 93270L.

[47] D.P. Jones, W. Hanna, G.M. Cramer, J.P. Celli, In situ measurement of ECM rheology and microheterogeneity in embedded and overlaid 3D pancreatic tumor stroma co-cultures via passive particle tracking, J. Innov. Opt. Health Sci. 10 (2017) 1742003.

[48] M. Daviran, S.M. Longwill, J.F. Casella, K.M. Schultz, Rheological characterization of dynamic remodeling of the pericellular region by human mesenchymal stem cell-secreted enzymes in well-defined synthetic hydrogel scaffolds, Soft Matter (2018).

[49] K.M. Schultz, K.A. Kyburz, K.S. Anseth, Measuring dynamic cell-material interactions and remodeling during 3D human mesenchymal stem cell migration in hydrogels, Proc. Natl. Acad. Sci. U. S. A. 112 (2015) E3757–E3764.

[50] J. Roether, S. Bertels, C. Oelschlaeger, M. Bastmeyer, N. Willenbacher, Microstructure, local viscoelasticity and cell culture suitability of 3D hybrid HA/collagen scaffolds, PLoS ONE 13 (2018) e0207397.

[51] P. Pawelzyk, N. Mücke, H. Herrmann, N. Willenbacher, Attractive interactions among intermediate filaments determine network mechanics in vitro, PLoS ONE 9 (2014) e93194.

[52] M. Votteler, P.J. Kluger, H. Walles, K. Schenke-Layland, Stem Cell Microenvironments-Unveiling the Secret of How Stem Cell Fate is Defined, Macromol. Biosci 10 (2010) 1302–1315.

[53] J.D. Mott, Z. Werb, Regulation of matrix biology by matrix metalloproteinases, Curr. Opin. Cell Biol. 16 (2004) 558–564.

[54] W. Cruz-Munoz, R. Khokha, The role of tissue inhibitors of metalloproteinases in tumorigenesis and metastasis, Critical reviews in clinical laboratory sciences 45 (2008) 291–338.

[55] R.J. McAnulty, Fibroblasts and myofibroblasts: Their source, function and role in disease, The International Journal of Biochemistry & Cell Biology 39 (2007) 666–671.

[56] L. Wang, Z.-y. Li, Y.-p. Wang, Z.-h. Wu, B. Yu, Dynamic expression profiles of marker genes in osteogenic differentiation of human bone marrow-derived mesenchymal stem cells, Chinese Medical Sciences Journal 30 (2015) 108–113.

[57] H.A. Declercq, R.M.H. Verbeeck, L.I.F.J.M. de Ridder, E.H. Schacht, M.J. Cornelissen, Calcification as an indicator of osteoinductive capacity of biomaterials in osteoblastic cell cultures, Biomaterials 26 (2005) 4964–4974.

[58] A. Procopio, E. Malucelli, A. Pacureanu, C. Cappadone, G. Farruggia, A. Sargenti, S. Castiglioni, D. Altamura, A. Sorrentino, C. Giannini, Chemical Fingerprint of Zn–Hydroxyapatite in the Early Stages of Osteogenic Differentiation, ACS Central Science 5 (2019) 1449–1460.

[59] A. Bouloumié, C. Sengenes, G. Portolan, J. Galitzky, M. Lafontan, Adipocyte produces matrix metalloproteinases 2 and 9: involvement in adipose differentiation, Diabetes 50 (2001) 2080–2086.

[60] J. Lilla, D. Stickens, Z. Werb, Metalloproteases and adipogenesis: a weighty subject, The American journal of pathology 160 (2002) 1551.

[61] W. Luo, H. Shitaye, M. Friedman, C.N. Bennett, J. Miller, O.A. MacDougald, K.D. Hankenson, Disruption of cell–matrix interactions by heparin enhances mesenchymal progenitor adipocyte differentiation, Exp. Cell Res. 314 (2008) 3382–3391.

[62] S. Khetan, M. Guvendiren, W.R. Legant, D.M. Cohen, C.S. Chen, J.A. Burdick, Degradation-mediated cellular traction directs stem cell fate in covalently crosslinked three-dimensional hydrogels, Nat. Mater. 12 (2013) 458–465.

[63] K.A. Marx, T. Zhou, A. Montrone, D. McIntosh, S.J. Braunhut, Quartz crystal microbalance biosensor study of endothelial cells and their extracellular matrix following cell removal: Evidence for transient cellular stress and viscoelastic changes during detachment and the elastic behavior of the pure matrix, Anal. Biochem. 343 (2005) 23–34.
[64] D. Gospodarowicz, C. Ill, Extracellular Matrix and Control of Proliferation of Vascular Endothelial Cells, J Clin Invest 65 (1980) 1351–1364.
[65] D.G. Stupack, D.A. Cheresh, ECM remodeling regulates angiogenesis: endothelial integrins look for new ligands, Sci. STKE 2002 (2002) pe7.
[66] M. Seandel, K. Noack-Kunnmann, D. Zhu, R.T. Aimes, J.P. Quigley, Growth factor-induced angiogenesis in vivo requires specific cleavage of fibrillar type I collagen, Blood 97 (2001) 2323–2332.
[67] K. Bieback, M. Vinci, S. Elvers-Hornung, A. Bartol, T. Gloe, M. Czabanka, H. Klüter, H. Augustin, P. Vajkoczy, Recruitment of human cord blood-derived endothelial colony-forming cells to sites of tumor angiogenesis, Cytotherapy 15 (2013) 726–739.
[68] W.H.O., Definition, diagnosis of diabetes mellitus and intermediate hyperglycemia: report of a WHO/IDF consultation, World Health Organization, Geneva, 2006, pp. 1–50.
[69] M.L. Gardel, M.T. Valentine, D.A. Weitz, Microrheology, in: K.S. Breuer (Ed.), Microscale diagnostic techniques, Springer, 2005, pp. 1–49.
[70] T.A. Waigh, Microrheology of complex fluids, Rep. Prog. Phys 68 (2005) 685–742.
[71] T.G. Mason, K. Ganesan, J.H. van Zanten, D. Wirtz, S.C. Kuo, Particle Tracking Microrheology of Complex Fluids, Phys. Rev. Lett 79 (1997) 3282–3285.
[72] T.G. Mason, Estimating the viscoelastic moduli of complex fluids using the generalized Stokes-Einstein equation, Rheologica Acta 39 (2000) 371–378.
[73] D. Wirtz, Particle-Tracking Microrheology of Living Cells: Principles and Applications, Annu. Rev. Biophys 38 (2009) 301–326.
[74] T. Indei, J.D. Schieber, A. Córdoba, E. Pilyugina, Treating inertia in passive microbead rheology, Phys. Rev. E Stat. Nonlin. Soft Matter Phys 85 (2012) 21504.
[75] L. van Hove, Correlations in Space and Time and Born Approximation Scattering in Systems of Interacting Particles, Physical Review 95 (1954) 249.
[76] E.R. Weeks, J.C. Crocker, A.C. Levitt, A. Schofield, D.A. Weitz, Three-Dimensional Direct Imaging of Structural Relaxation Near the Colloidal Glass Transition, Science 287 (2000) 627.
[77] T. Savin, P.S. Doyle, Statistical and sampling issues when using multiple particle tracking, Phys. Rev. E 76 (2007).
[78] V.F. Achterberg, L. Buscemi, H. Diekmann, J. Smith-Clerc, H. Schwengler, J.-J. Meister, H. Wenck, S. Gallinat, B. Hinz, The nano-scale mechanical properties of the extracellular matrix regulate dermal fibroblast function, Journal of Investigative Dermatology 134 (2014) 1862–1872.
[79] K.M. Schultz, K.S. Anseth, Monitoring degradation of matrix metalloproteinases-cleavable PEG hydrogels via multiple particle tracking microrheology, Soft Matter 9 (2013) 1570–1579.
[80] J. Gaffney, I. Solomonov, E. Zehorai, I. Sagi, Multilevel regulation of matrix metalloproteinases in tissue homeostasis indicates their molecular specificity in vivo, Matrix Biology 44 (2015) 191–199.
[81] D. Hanjaya-Putra, J. Yee, D. Ceci, R. Truitt, D. Yee, S. Gerecht, Vascular endothelial growth factor and substrate mechanics regulate in vitro tubulogenesis of endothelial progenitor cells, J Cellular Mol Med 14 (2010) 2436–2447.
[82] J. Xie, Q. Zhang, T. Zhu, Y. Zhang, B. Liu, J. Xu, H. Zhao, Substrate stiffness-regulated matrix metalloproteinase output in myocardial cells and cardiac fibroblasts: Implications for myocardial fibrosis, Acta Biomaterialia 10 (2014) 2463–2472.
[83] A.I. Caplan, Mesenchymal stem cells, Journal of orthopaedic research 9 (1991) 641–650.
[84] K.A. Kilian, B. Bugarija, B.T. Lahn, M. Mrksich, Geometric cues for directing the differentiation of mesenchymal stem cells, PNAS 107 (2010) 4872–4877.
[85] K.H. Vining, D.J. Mooney, Mechanical forces direct stem cell behaviour in development and regeneration, Nature Reviews Molecular Cell Biology 18 (2017) 728.
[86] A.M. Handorf, Y. Zhou, M.A. Halanski, W.-J. Li, Tissue stiffness dictates development, homeostasis, and disease progression, Organogenesis 11 (2015) 1–15.
[87] N.A. Ansari, Z. Rasheed, Non-enzymatic glycation of proteins: from diabetes to cancer, Biochemistry (Moscow) Supplement Series B: Biomedical Chemistry 3 (2009) 335.
[88] K.J. Welsh, M.S. Kirkman, D.B. Sacks, Role of glycated proteins in the diagnosis and management of diabetes: research gaps and future directions, Diabetes care 39 (2016) 1299–1306.
[89] T. Teissier, É. Boulanger, The receptor for advanced glycation end-products (RAGE) is an important pattern recognition receptor (PRR) for inflammaging, Biogerontology (2019) 1–23.
[90] Y. Liu, C. Liang, X. Liu, B. Liao, X. Pan, Y. Ren, M. Fan, M. Li, Z. He, J. Wu, AGEs increased migration and inflammatory responses of adventitial fibroblasts via RAGE, MAPK and NF-κB pathways, Atherosclerosis 208 (2010) 34–42.
[91] H. Dandia, K. Makkad, P. Tayalia, Glycated collagen–a 3D matrix system to study pathological cell behavior, Biomaterials science 7 (2019) 3480–3488.
[92] A. Lapolla, P. Traldi, D. Fedele, Importance of measuring products of non-enzymatic glycation of proteins, Clinical biochemistry 38 (2005) 103–115.
[93] N.C. Avery, A.J. Bailey, The effects of the Maillard reaction on the physical properties and cell interactions of collagen, Pathologie Biologie 54 (2006) 387–395.
[94] V.P. Singh, A. Bali, N. Singh, A.S. Jaggi, Advanced glycation end products and diabetic complications, The Korean Journal of Physiology & Pharmacology 18 (2014) 1–14.
[95] D. Baltzis, I. Eleftheriadou, A. Veves, Pathogenesis and treatment of impaired wound healing in diabetes mellitus: new insights, Advances in therapy 31 (2014) 817–836.
[96] J. Michaelson, V. Hariharan, H. Huang, Hyperglycemic and hyperlipidemic conditions alter cardiac cell biomechanical properties, Biophysical Journal 106 (2014) 2322–2329.
[97] D. Tousoulis, N. Papageorgiou, E. Androulakis, G. Siasos, G. Latsios, K. Tentolouris, C. Stefanadis, Diabetes mellitus-associated vascular impairment: novel circulating biomarkers and therapeutic approaches, Journal of the American College of Cardiology 62 (2013) 667–676.
[98] P.B. Pal, H. Sonowal, K. Shukla, S.K. Srivastava, K.V. Ramana, Aldose reductase regulates hyperglycemia-induced HUVEC death via SIRT1/AMPK-α1/mTOR pathway, Journal of molecular endocrinology 63 (2019) 11–25.
[99] M. Brownlee, The pathobiology of diabetic complications: a unifying mechanism, Diabetes 54 (2005) 1615–1625.
[100] S.-Y. Goh, M.E. Cooper, The role of advanced glycation end products in progression and complications of diabetes, The Journal of Clinical Endocrinology & Metabolism 93 (2008) 1143–1152.
[101] C. Rask-Madsen, G.L. King, Vascular complications of diabetes: mechanisms of injury and protective factors, Cell metabolism 17 (2013) 20–33.